Potassium Treatments for Solution-Processed Cu(In,Ga)(S,Se)₂ Solar Cells

Essam H. Alruqobah and Rakesh Agrawal*

Davidson School of Chemical Engineering, Purdue University
480 Stadium Mall Dr., West Lafayette, IN 47907, United States

*Corresponding author: agrawalr@purdue.edu

Keywords: CIGS, Cu(In,Ga)(S,Se)₂, alkali treatment, chalcopyrite solar cell, solution-processed solar cells, sodium fluoride, potassium fluoride

Abstract

Cu(In,Ga)(S,Se)₂ (CIGSe, CIGSSe) has emerged as an attractive thin-film solar cell absorber material owing to its high light absorption coefficient and tunable bandgap. In CIGSSe processing and fabrication, the use of alkali treatments has been implemented as sodium doping is considered a requirement for high efficiency CIGSSe solar cell devices and has been used extensively. One of the more significant developments in recent years has been the discovery of the beneficial effects that potassium post-deposition treatments have on vacuum-processed CIGSSe solar cells as they are responsible for a major increase in CIGSSe solar cell performance. Here, we conduct a study of the effect of potassium treatments to solution-processed CIGSSe films grown from colloidal sulfide-based nanoparticle inks. By adding potassium through e-beam evaporation of KF prior to selenization and grain growth, we find that the grain growth of CIGSSe is enhanced with potassium addition and that a larger-grained film results compared to untreated selenized CIGSSe film, similar to what is observed in sodium-treated films. We also observe through XPS that films treated with K show the presence of the high-bandgap K-In-Se surface phase. Fabricating devices, we find that films that have been subjected simultaneously to both sodium and potassium treatments have enhanced optoelectronic performance mainly manifested in higher open-circuit voltage and higher short-circuit current.

Introduction

Cu(In,Ga)(S,Se)₂ (CIGSSe) is one of the most promising thin-film solar cell materials with efficiencies reaching 23.35%, narrowing the gap towards conventional Si solar cells.¹ High-efficiency CIGSSe solar cells have been achieved mainly through the use of expensive vacuum-based processes such as co-evaporation and sputtering.^{2–5} To mitigate some of the costs associated with vacuum-based CIGSSe, solution-processed CIGSSe have gained interest as a more scalable and a less resource-intensive route towards thin film CIGSSe solar cells^{6–8}; today, solution-processed CIGSSe have reached 18% efficiency through the use of a hydrazine-based process.⁹

Achieving high-efficiency CIGSSe solar cells has required the use of alkali treatments. 8,10,11 Sodium treatment for CIGSSe has been utilized extensively in improving device performance and efficiency, both in vacuum-based routes 10,12, and in solution-processing routes.^{7,8,13} Sodium is known to enhance the performance of CIGSSe solar cell through passivation of grain boundaries and increased carrier density. 10,14-16 Moreover, If supplied before or during CIGSSe growth, Na also enhances grain growth of the absorber layer (e.g. when CIGSSe is grown on SLG substrates). 17,18 Other alkalis such as potassium, lithium, and cesium were thought to act in a similar manner as sodium. 19,20 However, one of the significant developments in CIGSSe processing in recent years has been the discovery the effects that heavy alkali (K, Rb, Cs) postdeposition treatments have in improving the performance of CIGSSe solar cells.^{1,21–23} Chirilă et al. have shown that unlike sodium, potassium added through a post-deposition treatment modifies the absorber surface by inducing the depletion of Cu and Ga from the surface and rendering it Cu and Ga poor, thereby enhancing Cd diffusion into the CIGSSe surface during CdS chemical bath deposition.²¹ This ultimately leads to an improvement of the junction quality and allows the deposition of a thinner CdS buffer layer without significant loss of V_{oc} or FF. ²¹ Moreover, reports

in the literature have observed surface bandgap widening for CIGSSe films subjected to a KF-PDT or NaF/KF-PDT treatments. ^{24,25} Pistor et al. have attributed the surface bandgap widening to be a result of a Cu-depleted film surface. ²⁵ However, other reports in the literature have shown that a high bandgap In₂Se₃ or KInSe₂ surface phase forms on the CIGSe absorbers subjected to a KF-PDT treatment, and that this surface phase is responsible for the increased surface bandgap observed for KF-treated CIGSe. ^{24,26–28} The increased surface bandgap enhances junction quality and reduces interface recombination. ²⁸ Despite these very beneficial effects of potassium treatments, they have only been applied to vacuum-based CIGSSe solar cells, and to the best of our knowledge no report on the systematic use of K treatments on solution-processed CIGSSe devices is published. Guo et al. used potassium cyanide treatments on CIGS nanoparticle films prior to selenization to render them Cu-poor and observed performance improvements. ⁸

In this work, the effects of potassium treatments on solution-processed CIGSSe films is explored through the use of potassium fluoride as the K source. First, we study the effects potassium has on the morphology and grain size of the absorber films. Next, we show how the potassium alters the surface chemistry of the CIGSSe absorber film using XPS where it is found to cause the formation of an additional Se surface state not present in non-treated films or NaF-only treated films. Finally, the optoelectronic performance of CIGSSe solar cells in terms of J-V parameters, EQE, and carrier concertation with varying potassium and/or sodium content is evaluated. We find that, like sodium, potassium enhances the growth of CIGSSe grains from CIGS and leads to a larger grained film. Additionally, we find that K-treated films show enhanced optoelectronic performance manifested in higher open-circuit voltage and fill factor, as compared to non-treated and Na-only treated films.

Experimental Section

Cu(In,Ga)Se₂ films are selenized from Cu(In,Ga)S₂ nanoparticle films as outlined below.

Nanoparticle Film Formulation and Alkali Addition

Cu(In,Ga)S₂ nanoparticles were synthesized via a solvo-thermal/hot-injection reaction of a sulfur solution and Cu,In, and Ga salts, as outlined by McLeod et al and Guo et al. ^{7,8} Briefly, a 1.0 M sulfur (Sigma-Aldrich, 99.99%) in degassed oleylamine (Sigma Aldrich, reagent grade 70%, ≥ 98% primary amines) solution is prepared in a N₂-filled glovebox by adding sulfur flakes in oleylamine-containing flask which was sealed in the glovebox. The S-OLA was heated at 65 °C for 1 hour to ensure complete dissolution of sulfur in the oleylamine. The metals-OLA solution is prepared by adding 1.38 mmol Cu(II) acetylacetonate (Sigma Aldrich, 99.9%), 1.5 mmol In acetylacetonate (Sigma Aldrich, 99.99%), and 0.45 mmol Ga acetylacetonate (Sigma Aldrich, 99.99%) to 12 ml of oleylamine in a nitrogen-filled glovebox. The metals-OLA flask is taken out of the glovebox and preheated to 285°C under inert argon. Upon reaching 285°C, the 1.0 M sulfur-OLA solution is injected into the metal salts-OLA flask. The reaction was allowed to proceed for 30 minutes at 285°C under Ar atmosphere. Following the reaction, the nanoparticles were washed in hexane and alcohols to remove excess OLA and unreacted precursors. The as-coated Cu(In,Ga)S₂ nanoparticle film had a [Cu]/[In]+[Ga] of 0.92 ± 0.02 , and [Ga]/[In]+[Ga] of 0.27 ± 0.02 0.01, as measured by XRF.

The synthesized Cu(In,Ga)S₂ nanoparticles were then suspended in hexanethiol forming the colloidal nanoparticle ink. The ink was then coated onto Mo-coated soda-lime glass substrates via blade-coating technique and annealed at 300°C to evaporate excess organic material. No intentional Ga grading was applied.

Sodium and potassium were supplied by evaporating NaF (Sigma Aldrich, 99.99%) and KF (Sigma Aldrich, 99.9%) onto the as-coated sulfide CIGS nanoparticle film, or the as-selenized CIGSSe films, via e-beam evaporation. No KCN treatment was used.

Absorber Selenization And Growth

Cu(In,Ga)S₂ (CIGS) nanoparticle films were selenized and grown into Cu(In,Ga)(S.Se)₂ (CIGSSe) grains in a tubular furnace under a Se-argon atmosphere. The nanoparticle film is placed in a rectangular graphite box along with Se pellets and annealed at 500 °C for 20 minutes under inert argon. The graphite box was then allowed to cool naturally to room temperature, also under an argon atmosphere. The selenized CIGSSe films have a [Cu]/[In]+[Ga] of 0.87 ± 0.02 , and [Ga]/[In]+[Ga] of 0.26 ± 0.01 , as measured by XRF.

Solar Cell Fabrication

CIGSSe solar cells were fabricated using the conventional stack SLG/Mo/CIGSSe/CdS/i-ZnO/ITO/Ni-Al grids. 50 nm thick CdS n-type buffer layer was deposited via chemical-bath deposition. This is followed by deposition of 80 nm i-ZnO and 220 nm of indium-doped tin oxide (ITO) TCO layers using radio frequency (RF) sputtering. Devices were finished by evaporation of Ni-Al grids using e-beam evaporation. Individual cells were isolated via mechanical scribing, with each cell area having a nominal area of 0.47 cm². Unless otherwise stated, all devices shown have 100 nm MgF₂ anti-reflective coating deposited via e-beam evaporation.

Characterizations

Elemental ratios were measured using a Fischerscope XAN 250 X-ray fluorescence instrument. Plan-view and cross-sectional scanning electron images were taken using a FEI Quanta electron microscope under an accelerating voltage of 10 keV. Grain size analysis and quantification of each alkali condition was conducted on the SEM plan view images by first

identifying individual grains using edge detection in Adobe Photoshop, and then using ImageJ image processing software²⁹ to produce average grain area and grain perimeter distributions, as shown by McLeod et al.¹⁸ Grain diameters were calculated by assuming circular grains using the relation Grain Diameter = 4*(Grain Area)/(Grain Perimeter).¹⁸

Powder X-ray diffraction data was collected in Bragg-Brentano mode using a Rigaku SmartLab diffractometer with a Cu Kα radiation source. Raman spectroscopy data was collected using a Horiba/John Yvon HR800 confocal microscope using a 633 nm He:Ne laser with 100x magnification.

X-ray photoelectron spectroscopy (XPS) data was collected on the selenized CIGSSe films at the Surface Analysis Facility of the Birck Nanotechnology Center, Purdue University using a Kratos AXIS Ultra DLD Imaging X-ray Photoelectron Spectrometer, with a monochromatic Al $K\alpha$ (1486.6 eV) radiation and a chamber base pressure of less than 2 \times 10⁻⁹ Torr. To minimize oxygen surface contamination after selenization, samples were transferred rapidly from the selenization furnace to a N₂-filled glovebox with a transfer time of less than 1 minute. Samples were then soaked in dilute ammonia solution in the glovebox to remove excess alkali and alkali fluorides from the surface, after which they were then dried with nitrogen and vacuum sealed inside the glovebox for transfer to the XPS instrument. The vacuum seal was broken in an inert glovebox connected to the XPS instrument with a load-lock chamber through which the samples were loaded into the XPS chamber. XPS photoelectron peak analysis and fitting was done using CasaXPS software with Voigt profiles and a linear background. The adventitious carbon C 1s peak is set to 285 eV. Spin-orbit doublets' FWHM of respective Voigt profiles are set equal and the peak area is fixed according to corresponding |2j + 1| multiplicity of each orbital.³⁰ All XPS spectra were area normalized to the Se 3d peak area of each respective sample.

Solar Cell Characterization

Four-point probe current-voltage (J-V) measurements were conducted under standard AM1.5 conditions using an Oriel Sol3A solar simulator calibrated to 1000 W/cm² using an Oriel 91150 V silicon reference cell. All J-V measurements were conducted at 25 °C using a temperature-controlled stage. J-V data was analyzed according to methods provided by Hegedus and Shafarman. External quantum efficiency (EQE) data was taken at zero bias using an in-house built instrument with a preamplifier and lock-in amplifier for signal processing with a chopper frequency of 160 Hz. Capacitance-voltage profiling was conducted using an Agilent 4284A impedance analyzer. Capacitance-voltage data was collected on completed devices under dark conditions at room temperature at 100 kHz AC frequency and 2 mV_{RMS}.

Results

To elucidate the effect potassium has on the morphology of the film, nanoparticle films with no alkali, 10 nm, 20 nm, and 50 nm evaporated KF were selenized at 500°C for 20 minutes with excess Se, as discussed in the experimental section.

Figure 1 shows the SEM plan view and cross-sectional images of the selenized absorber films with different amounts of evaporated KF prior to selenization, and Figure 2(a) shows the average grain diameter of CIGSSe films selenized with different KF amounts. The CIGSSe grain size and morphology are affected by the amount of potassium that is evaporated onto the film with the grain size and coarsened film thickness increase with the amount of KF added to the film prior to selenization. The plan view images (Figure 1, left column) and average grain diameter (Figure 2(a)) show the film grain size gradually increasing with increasing KF amount. Moreover, a simultaneous decrease of the underlying 'fine grain' layer thickness is also observed. Increasing the evaporated KF thickness to 50 nm shows CIGSSe grains starting to separate into islands, with

pinholes between them exposing the fine grain layer underneath. (Figure 1 (g-h)). The fine grain layer is typically observed for solution-processed CIGSSe and CZTSSe absorber films. ^{13,18,32,33} The origin of this layer is primarily due to the carbon leftover from carbon-containing ligands and reagents that are used during the processing steps prior to selenization. ^{13,32,34–36}

The potassium effect on the growth morphology and grain size is similar to what is seen with sodium in CIGSe^{8,17,18} and in CZTSSe.³⁷ To compare the effects between Na and K treatments, CIGSSe films were selenized with 5 nm, 10 nm, 15 nm, and 30 nm of NaF evaporated prior to selenization; Figure S1 shows the SEM plan-view and cross-sectional images of those CIGSSe films, while Figure 2(b) shows the measured average grain diameter. Films treated with NaF show larger grain sizes and a thicker coarsened layer than films treated with a similar thickness of KF; the selenized grain film thickness with 10 nm NaF (Figure 2 (b); Figure S1 (b),(f)) is larger than in the 10 nm KF film (Figure 1 (c), (d); Figure 2 (a)). Moreover, the film that was selenized with 30 nm NaF has comparable average grain size (Figure 2 (a), (b)) as the 50 nm KF sample with a similar island morphology and pinholes exposing the carbonaceous fine grain (Figure 1 (g,h). For the same evaporated thickness, NaF is more active than KF in enhancing the grain growth and sintering of CIGSSe films. The higher activity of sodium over heavier alkalis (K, Cs) in enhancing the grain growth has also been observed in vacuum-based CIGSe grown via coevaporation.²⁰

Braunger et al. have proposed that Na enhances growth because it enhances selenium incorporation in the film.³⁸ Sodium is proposed to bind to vapor selenium and forms a liquid Na₂Se_x which has a higher sticking coefficient than Se.³⁸ Furthermore, Na₂Se_x segregates at grain boundaries and will act as a liquid reservoir for selenium during growth.³⁸ Presence of liquid Na₂Se_x during growth also provides an enhanced medium for elemental diffusion, which will assist

sintering and grain growth. 39,40 McLeod et al. have investigated the effect of Na on the growth of CIGSSe films from a CIGS nanoparticle precursor and have hypothesized than Na present during growth will assist with Cu, In, and Ga diffusion, which otherwise would be limited, by forming a liquid flux agent in the film. As for potassium, no mechanism regarding its ability to impact the grain growth of CIGSe (CIGSSe) from a nanoparticle film has been reported in the literature. Results in Figure 1 and Figure 2 (a) show that the final CIGSSe grain size correlates with how much K is in the film with a similar trend observed for Na-treated films (Figure 2 (b) and Figure S1). Moreover, the same trend was observed for films selenized with both NaF and KF treatments. Figure 3 shows SEM plan-view and cross-sectional images of CIGSSe films treated with both Na and K, while Figure 2(c) shows the average grain diameter. Adding Na, K, or both assists in the growth of the film and leads to a film with larger grain size. Since similar effects on the morphology are observed in NaF and KF-treated films, it is likely that K acts in a comparable mechanism as Na in terms of its effect on the growth of CIGSSe films. Figure S2 (a), (b), and (c) in the Supporting Information show the PXRD patterns of the selenized films with different alkali contents; and Figure S2 (d) shows the Raman spectra of the films selenized with different KF amounts. A broad shoulder to the left of CIGSe Raman A1 mode at ~ 155 cm⁻¹ is detected for 20 nm KF-treated film, which is characteristic of the ordered defect complex (ODC). The ODC has lower Cu content than Cu(In,Ga)Se₂ chalcopyrite structure. 13,41,42

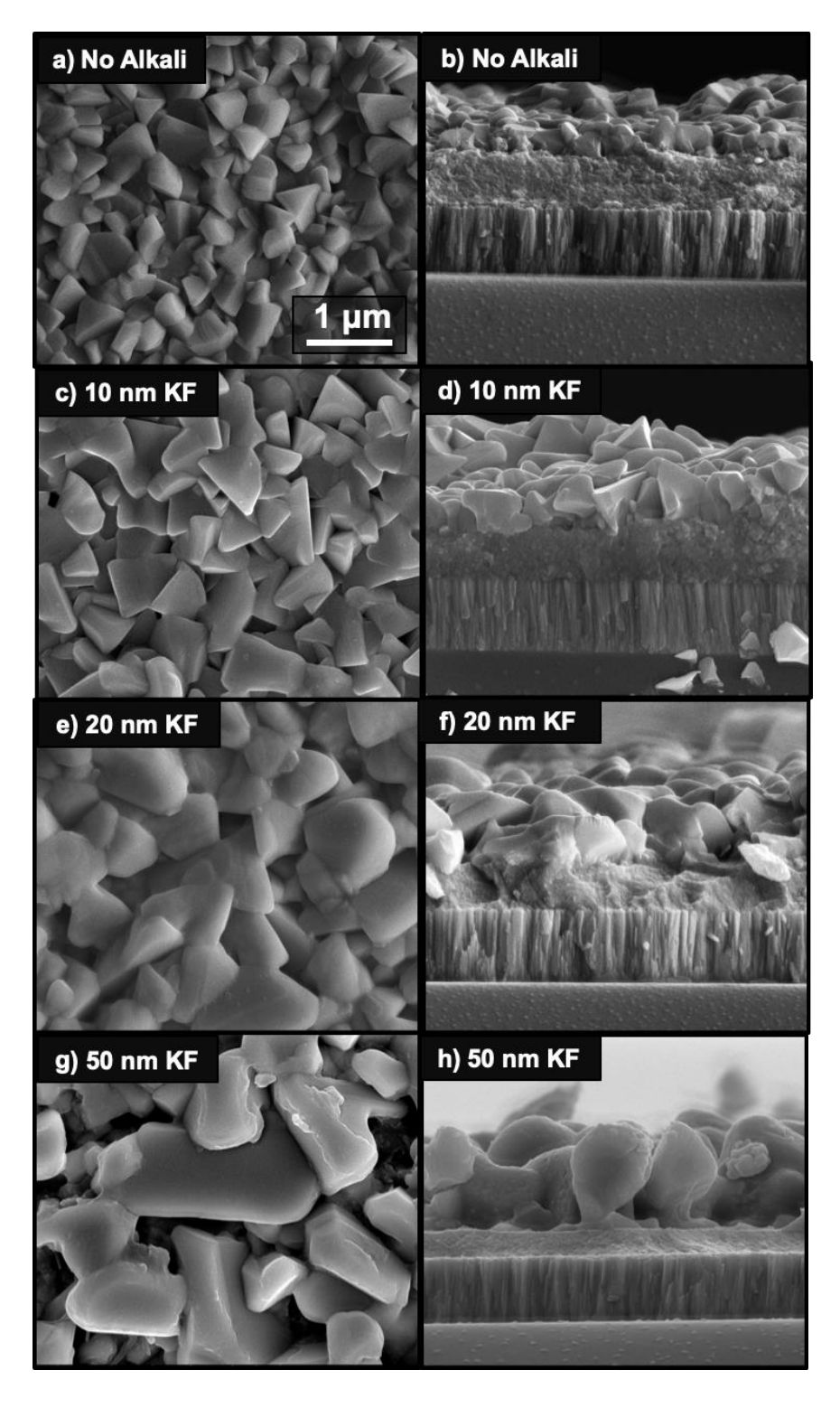


Figure 1: SEM plan-view (a,c,e,g) and cross-sectional (b,d,f,h) images of $Cu(In,Ga)(S,Se)_2$ films selenized at $500^{\circ}C$ for 20 minutes with no alkali addition (a-b), 10 nm KF (c-d), 20 nm KF (e-f), and 50 nm KF (g-h). Scale bar is same for all images.

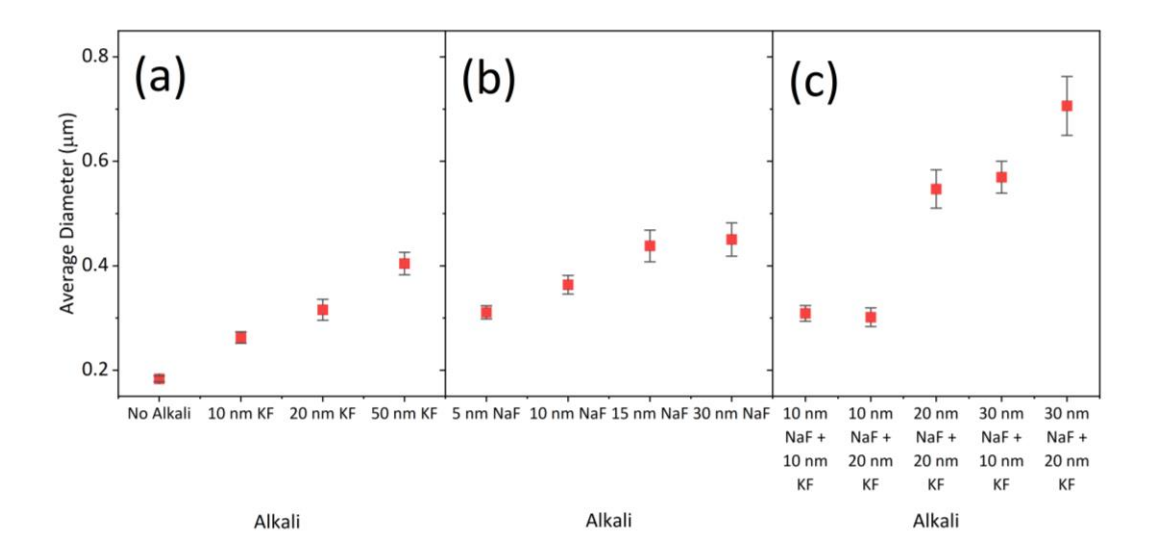


Figure 2: Average grain diameter of CIGSSe films selenized at 500 °C for 20 minutes with (a) different KF amounts, (b) different NaF amounts, and (c) with different NaF amounts.

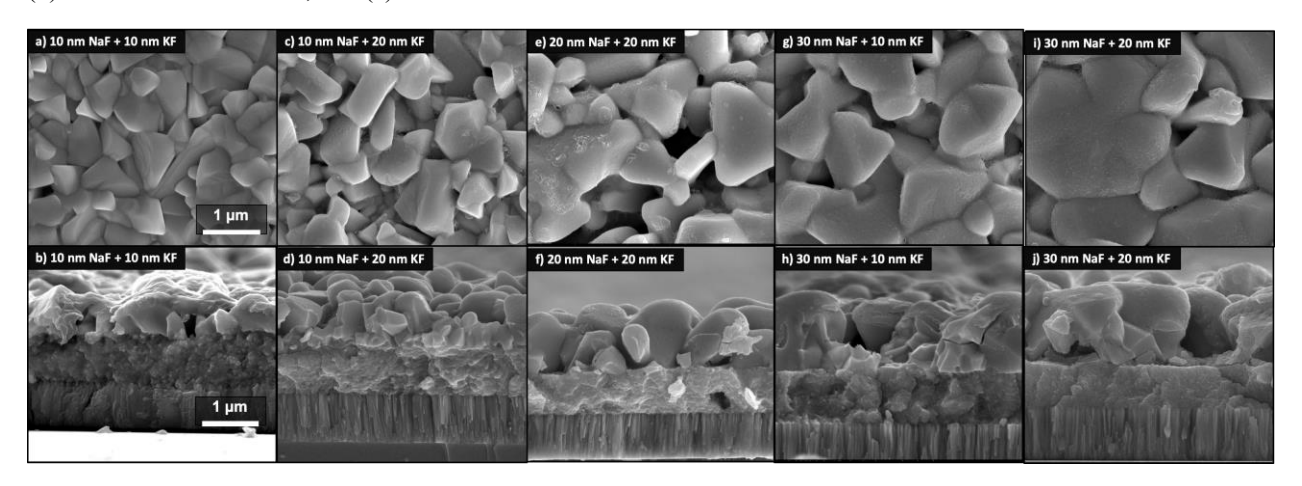


Figure 3: SEM plan-view and cross-sectional) images of $Cu(In,Ga)(S,Se)_2$ films selenized at 500 °C for 20 minutes with different NaF + KF combinations evaporated onto the as-coated film prior to selenization: 10 nm NaF + 10 nm KF (a-b), 10 nm NaF + 20 nm KF (c-d), 20 nm NaF + 20 nm KF (e-f), 30 nm NaF + 10 nm KF (g-h), and 30 nm NaF + 20 nm KF (i-j). Scale bar is same for all images.

The surface chemical environment of the selenized Cu(In,Ga)(S,Se)₂ films were also analyzed using X-ray photoelectron spectroscopy (XPS). Figure 4 shows the XPS data for the Se 3d core level for CIGSSe films selenized with different thicknesses of alkali fluorides deposited prior to selenization: without addition of alkali (No Alkali), 15 nm NaF, 10 nm KF, and 20 nm KF. Voigt peak fitting on the Se 3d XPS signal shows the presence of two Se 3d contributions (Se-1 and Se-2) for all samples. Se-1 and Se-2 signals have been suggested to belong to the CIGSe

chalcopyrite chemical environment.^{24,41,43,44} For the sample selenized with 20 nm KF, we were able to identify an additional minor Se 3d contribution (Se-3) at lower binding energy than the Se-1 and Se-2; the Se-3 is not observed in either the No Alkali, 15 nm NaF, or the 10 nm KF samples. This low-binding energy state is observed in vacuum-grown CIGSe subjected to a KF-PDT, and is attributed to a K-In-Se surface species.^{24,28,44} Handick et al. have shown that the K-In-Se widens the bandgap at the absorber surface markedly, and have suggested that this would aid in the passivation of the CIGSSe/CdS junction and that this surface state is one of the reasons for the increased performance of films treated with KF-PDT.²⁸ Figure 5 shows the XPS spectra of Se LMM-K 2p region. A shoulder on the Se LMM peak is observed on the lower binding energy side at ~293.7 eV for films selenized with evaporated KF, which is attributed to the K 2p_{3/2} photoelectron transition; associated Voigt peaks are also shown on Figure 5. Despite observing K on the surface of the 10 nm KF sample through XPS and the enhanced solar cell performance (see Solar Cell Performance section), we were not able to identify the Se-3 state with certainty in the Se 3d XPS core level spectrum for the 10 nm KF sample.

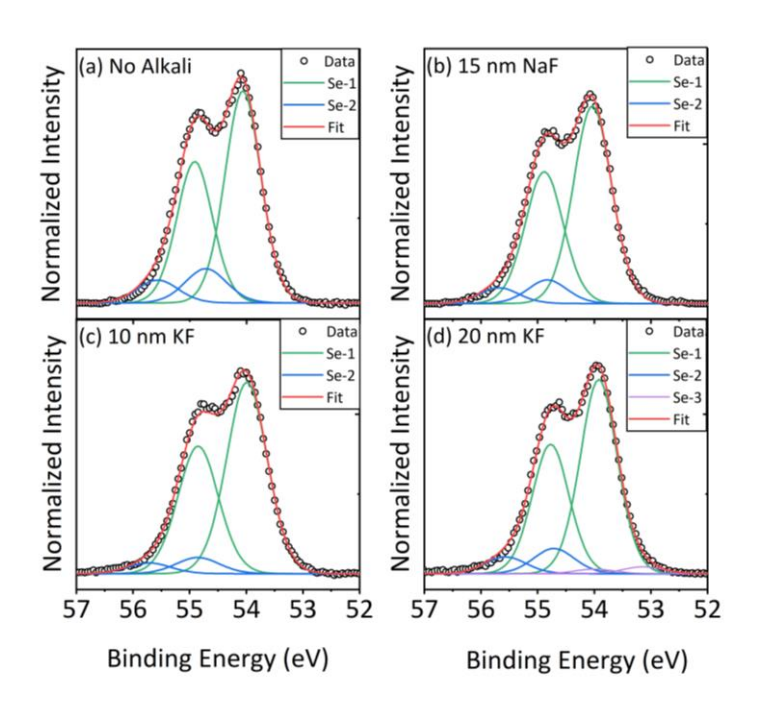


Figure 4: Normalized Se 3d XPS transitions of CIGSSe films selenized at 500 °C for 20 minutes with (a) no alkali added, with (b) 15 nm NaF, (c) with 10 nm KF, and (d) with 20 nm KF. When fitting the Se 3d doublet contribution, the Se $3d_{5/2}$ and $3d_{3/2}$ doublet separation was set at 0.86 eV.

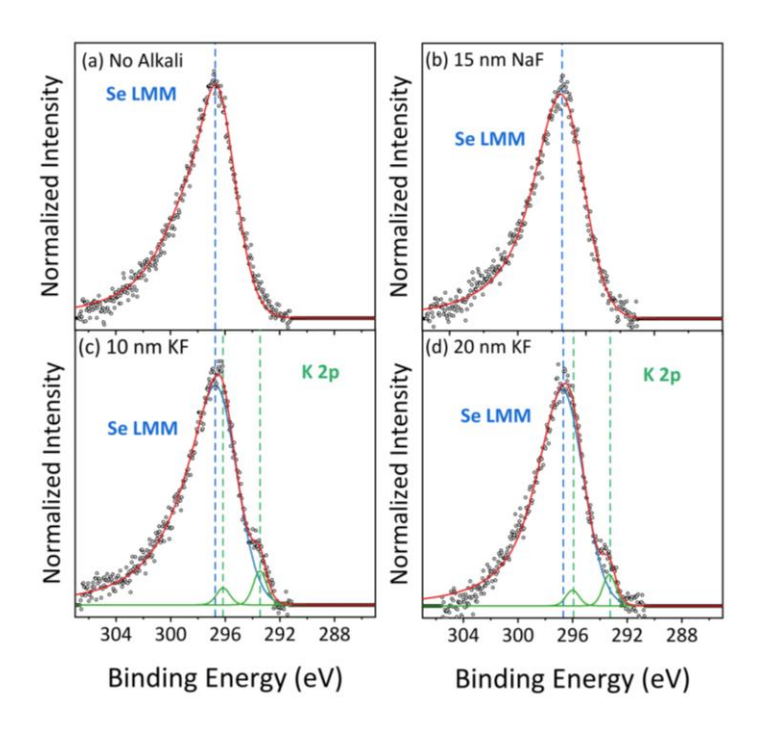


Figure 5: Normalized Se LMM Auger transition and K 2p photoelectron transitions of CIGSSe films selenized at 500 °C for 20 minutes with (a) no alkali added, (b) with 15 nm NaF, (c) with 10 nm KF, and (d) with 20 nm KF. K 2p doublet separation is set at 2.70 eV. K 2p peak is fitted with a Voigt profile, while the Se LMM Auger transitions was fitted with an asymmetric peak.

The indicated alkali amounts show the alkali that was added to the film prior to selenization. However, the films are deposited onto Mo-coated soda-lime glass so some Na diffusion from the glass is expected. Figure S3 in the Supporting Information shows the Na 1s XPS transitions. The No Alkali sample shows the lowest Na 1s peak intensity, with the 15 nm NaF unsurprisingly showing higher Na 1s intensity. The KF-only films (10 nm KF, 20 nm KF, and 25 nm KF) were not subjected to any external Na treatment and were selenized at the same temperatures and for the same duration as the other samples, with the only Na source for the KFonly samples being the SLG substrate. We would then expect the same amount of Na on the surface for the No Alkali and KF-only conditions. However, what we found was that the signal intensity of the Na 1s peak was higher for the 20 nm KF and the 25 nm KF conditions compared to the No Alkali condition. The fact that the only Na source is the SLG substrate and that the intensity of the Na 1s signal correlates with the amount of KF evaporated on the film suggests that K aids in the out-diffusion of Na from the glass substrate. Similar behavior was reported for Li-doped solutionprocessed CZTSSe films in which films with Li added to the ink showed more Na diffusion from the glass through an ion-exchange mechanism.⁴⁵

Figure 6 shows the normalized Cu 2p_{3/2}, In 3d_{5/2}, and Ga 2p_{3/2} XPS transitions for CIGSSe films selenized at 500 °C for 20 minutes with various alkali contents. Slight attenuation of the Cu 2p_{3/2} is observed with samples selenized with alkali fluorides evaporated prior to selenization (15 nm NaF, 10 nm KF, and 20 nm KF) compared to the No Alkali baseline condition. However, this attenuation is much less than what is reported in the literature for CIGSe grown with the 3-stage process where almost complete removal of Cu from the surface is observed.^{21,24} Furthermore, a minor attenuation is also observed for Ga for the 15 nm NaF and 20 nm KF conditions, as shown

in the Ga $2p_{3/2}$ XPS core level transition on Figure 6. The Ga attenuation is also much less than in the CIGSe absorber films made using the 3-stage process.^{21,24,41}

One of the beneficial effects of KF-PDT in vacuum-based CIGSe is that it induces the surface depletion of Ga and Cu.²¹ This facilitates Cd diffusion into the CIGSe film during the CdS chemical bath deposition, and in practice allows a thinner CdS layer.^{21,44} For the CIGSSe films that are selenized with KF-evaporated prior to selenization (Figure 6), the attenuation in Cu (10 nm KF and 20 nm KF conditions), and in Ga (20 nm KF condition) is minor and is significantly less than what is seen for CIGSe films grown subjected to a KF-PDT.^{21,24} A post-deposition treatment may be a necessary condition to induce Ga or Cu and Ga surface depletion. To investigate if this might be the case, we applied a KF treatment via e-beam evaporation to a selenized CIGSSe film (500°C, 20 minutes, 10 nm NaF evaporated prior to selenization) by evaporating 20 nm KF via e-beam evaporation on the as-selenized film followed by annealing the film at 300 °C under a Se atmosphere for 20 minutes (10 nm NaF + 20 nm KF PDT). The Cu 2p_{3/2}, In 3d_{5/2}, and Ga 2p_{3/2} XPS transitions are shown on Figure 6. Both Cu and Ga surface depletion for these films are observed, as well as an increase in the In 3d_{5/2} signal indicating that the surface is In rich. Additionally, a shift to higher binding energies for the Cu 2p_{3/2}, In 3d_{5/2}, and Ga 2p_{3/2} photoelectron spectra for the film that was subjected to KF PDT was observed. This shift may be attributed to the formation of an In-oxide and Ga-oxide species on the surface of the film. Lepetit et al. have shown that K or KF-induced rapid oxidation of co-evaporated CIGSe surface forming a stable In_xO_y on the surface of the film, and that further oxidation of the surface is not sensitive to air exposure time. 46 Furthermore, the low binding energy Se-3 surface state in Se 3d XPS transition was also observed for the film that underwent KF-PDT (Figure S5 in the Supporting Information), similarly to what was observed in Figure 4 (d) for films that were subjected to 20 nm KF treatment

prior to selenization. XPS transitions belonging to the K 2p core level were also observed for the 10 nm NaF + 20 nm KF PDT condition confirming that K is present on the surface (Figure S5 in the Supporting Information), which is similar to what was observed for the films that had KF evaporated prior to selenization (Figure 5 (c) and (d)). However, despite that NaF was evaporated on the as-coated film prior to selenization, no Na was detected on the surface of the 10 nm NaF + 20 nm KF PDT film (Figure S5 in Supporting Information). This is consistent with reports in the literature that show the removal of Na after KF-PDT. 41,46,47 Figure S4 in Supporting Information shows the SEM plan-view and cross-sectional images of the 10 nm NaF film after 20 nm KF-PDT.

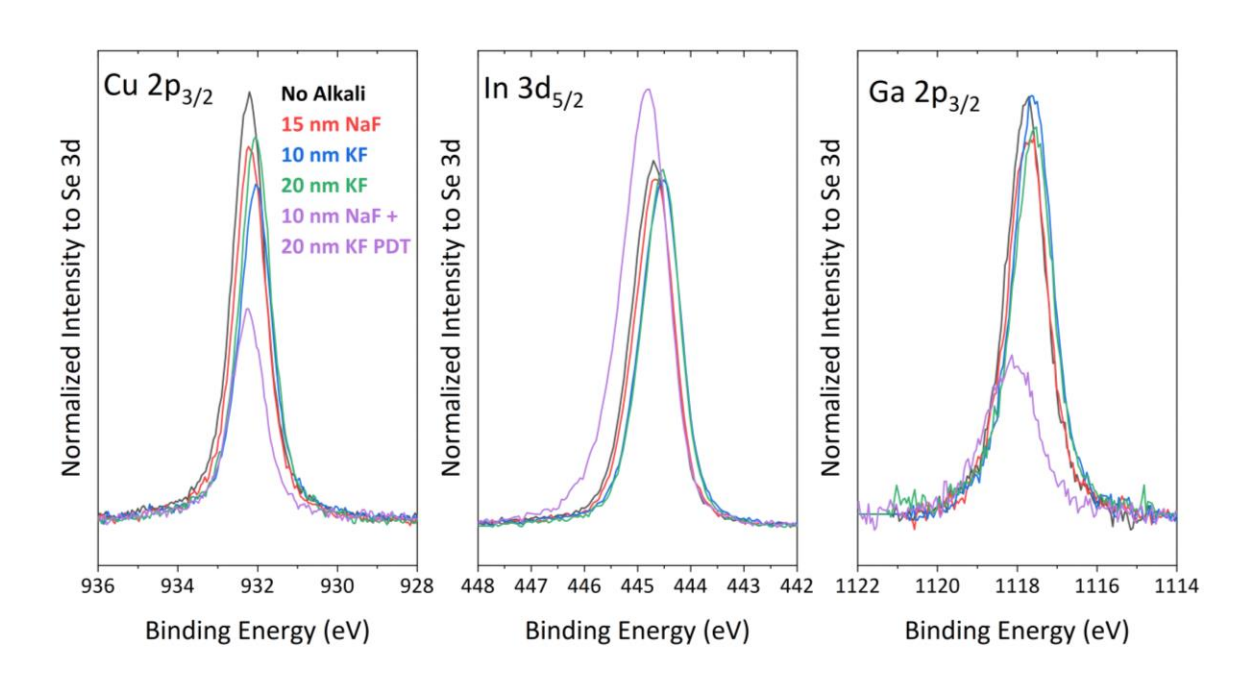


Figure 6: Cu $2p_{3/2}$, In $3d_{5/2}$, and Ga $2p_{3/2}$ XPS photoemission spectra of selenized CIGSSe films with no alkali added, 15 nm NaF, 10 nm KF, 20 nm KF, and 10 nm NaF + 20 nm KF PDT. All spectra are area-normalized to Se 3d of each respective sample.

Solar Cell Performance

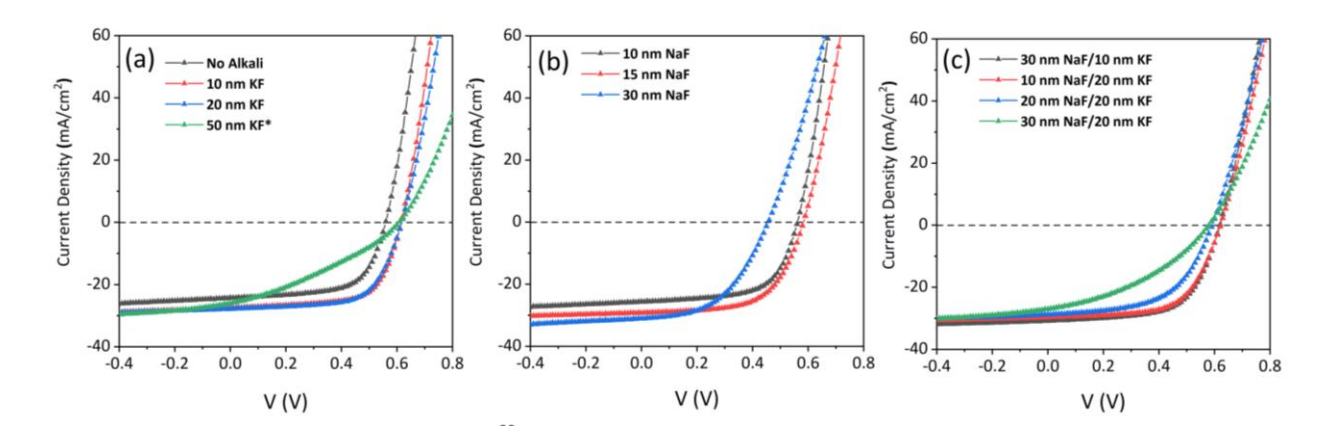


Figure 7: Illuminated J-V curves of CIGSSe devices with (a) different KF amounts, (b) different NaF amounts, and (c) different NaF/KF combinations. The alkali fluoride thicknesses given correspond to the evaporated thickness onto the nanoparticle film prior to selenization. * denotes samples without MgF₂ anti-reflective coating.

Devices were completed for the CIGSSe films that were selenized with the different alkali contents and the results are tabulated in Table 1. Figure 7 (a) shows the light J-V curves of films that were subjected to a pre-selenization KF treatment only. A significant increase in power conversion efficiency (p.c.e.) is observed, increasing from 8.8% for the No Alkali condition to 11.3% with only 10 nm KF, and to 11.2% for the 20 nm KF condition. The p.c.e. drops to 5.5% for the 50 nm KF condition. The major increase in efficiency is attributed to significant increase in the open circuit voltage Voc from 0.56 V for the No Alkali condition to 0.62 V for both 10 nm KF and 20 nm KF condition. Moreover, the 50 nm KF case exhibited an increased V_{oc} of 0.61 V over the No Alkali condition. We also observed an increase in the short circuit current density $J_{\rm sc}$ from 24.3 mA/cm² for the No Alkali case to 27.6 mA/cm² and 27.8 mA/cm² for the 10 nm KF and 20 nm KF cases, respectively; the 50 nm KF condition also had increase in $J_{\rm sc}$ to 27.2 mA/cm² without a MgF₂ anti-reflective coating. The fill factor showed a slight increase to 66% and 64.8% for the 10 nm KF and 20 nm KF conditions, respectively, compared to 64.4% the No Alkali condition. The drop in efficiency for the 50 nm KF is due to the significant drop in FF (33.3%). The reason for the drastic drop in FF for the 50 nm KF case is not entirely clear at this point, but barrier formation as a result of excess K is suspected. Formation of a barrier for injection current has been shown to form as a result of KF-PDT.⁴⁸ Moreover, current barrier formation has also been observed for CIGSe films treated with excess Rb.^{22,49,50}

To further explore the effect of alkali on the performance of nanoparticle-based CIGSSe, we also fabricated devices with different NaF treatments prior to selenization. Figure 7 (b) shows the light JV curves for NaF-treated devices. An increase in the p.c.e. is also observed with Na, but less drastic than KF-treated films, with an increase in the p.c.e. to 9.3 % and 10.7% for the 10 nm NaF and 15 nm NaF, respectively. The increase in V_{oc} is more subtle for the NaF-treated films than the K-treated films, with an increase to 0.59 V for the 15 nm NaF case only. A decrease in FF with increasing NaF thickness is also observed, with the FF decreasing to 53.1% for the 30 nm NaF case which may be a consequence of the pinhole film morphology as seen in the SEM plan view images (Figure S1 (d)). The results above suggest that KF treatments improves the V_{oc} more than NaF treatments, while NaF treatments are more effective in improving the J_{sc} .

CIGSSe solar cells were also fabricated with both NaF and KF treatments. Figure 7 (c) shows the light J-V curves for CIGSSe films subjected to both NaF and KF treatments. An efficiency boost was obtained for the cases of both NaF and KF were evaporated with a p.c.e. of 12.0% for the case in which 30 nm NaF+10 nm KF were evaporated prior to selenization. The 10 nm NaF+20 nm KF case also exhibited efficiency increase to 11.6%. Both of these conditions exhibited significant increases in both the V_{oc} and the J_{sc} as compared to the No Alkali case. A significant drop in FF is also observed with increasing alkali content for the NaF+KF cases, with the FF dropping to 55.7% and 36.7% for the 20 nm NaF+20 nm KF and the 30 nm NaF+20 nm KF conditions, respectively.

The 10 nm NaF CIGSSe film subjected to 20 nm KF-PDT showed detrimental optoelectronic performance with a p.c.e. of 4.9% (Table 1 and Figure S6), compared to a p.c.e. of 9.3% for the 10 nm NaF condition without the KF-PDT. The reason for the sharp drop in optoelectronic performance is not clear at this point. Detrimental performance as a result of KF-PDT has been reported for three-stage co-evaporated CIGSe when grown under certain conditions. The effect of potassium post-selenization treatment and its optimization for solution-processed CIGSSe absorbers is currently an area of study.

Series and shunt resistances for the different alkali conditions are tabulated in Table S1 in the Supporting Information, and dark J-V curves for key samples are shown in Figure S7 in the Supporting Information.

Table 1:Performance parameters for CIGSSe devices selenized with the different alkali contents. * denotes devices without MgF₂ anti-reflective coating. All efficiencies are based on total cell area.

Condition	η (%)	V _{oc} (V)	J _{sc} (mA cm ⁻²)	FF (%)
No Alkali	8.8	0.56	24.3	64.4
10 nm KF	11.3	0.62	27.6	66.0
20 nm KF	11.2	0.62	27.8	64.8
50 nm KF*	5.5	0.61	27.2	33.3
10 nm NaF	9.3	0.56	25.6	64.4
15 nm NaF	10.7	0.59	29.2	62.3
30 nm NaF	8.1	0.49	31.0	53.1
30 nm NaF + 10 nm KF	12.0	0.62	30.8	62.6
10 nm NaF + 20 nm KF	11.6	0.62	29.6	63.3
20 nm NaF + 20 nm KF	9.5	0.59	28.9	55.7
30 nm NaF + 20 nm KF	6.0	0.59	27.8	36.7
10 nm NaF + 20 nm KF PDT*	4.9	0.57	20.4	42.4

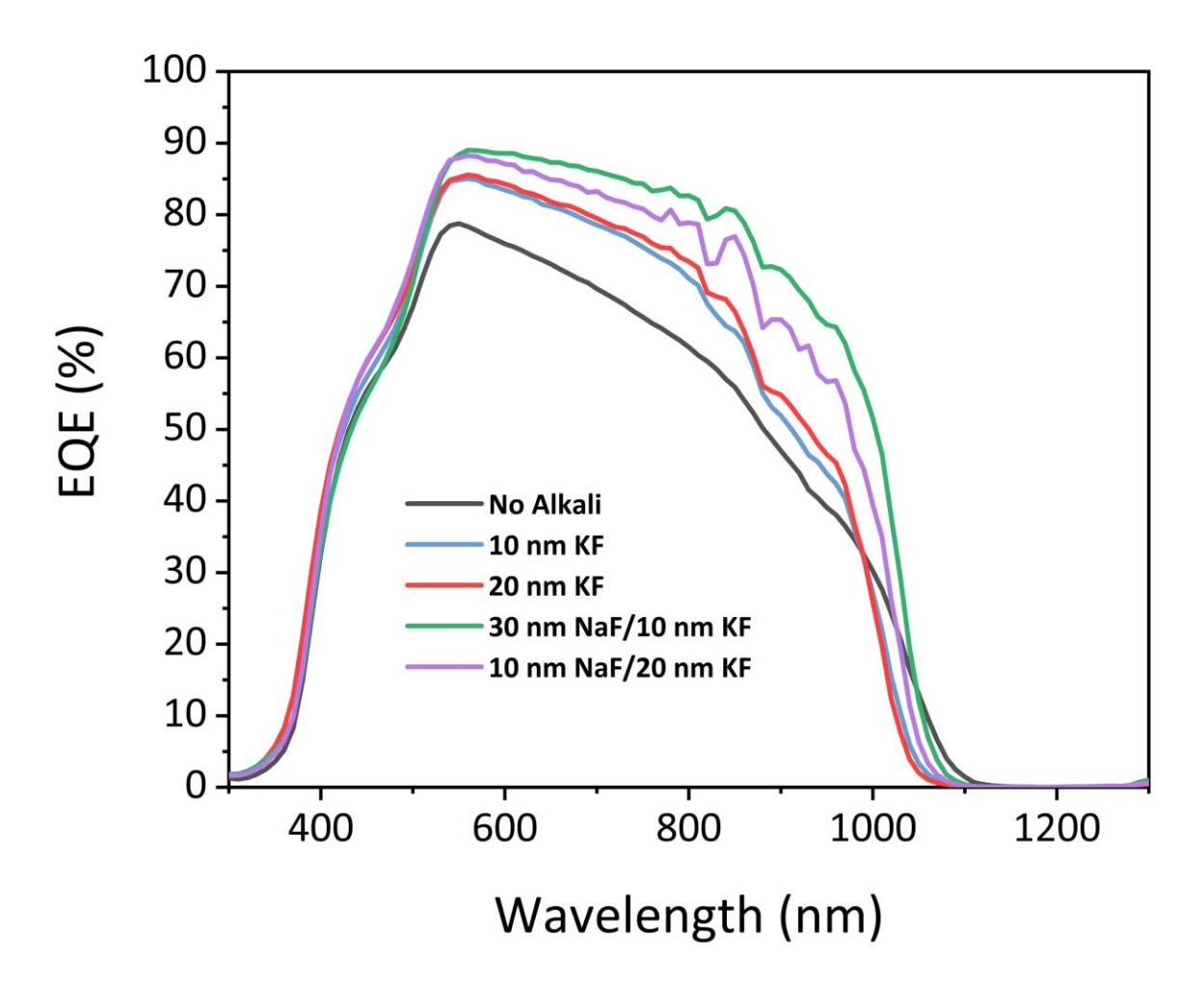


Figure 8: EQE measurements of CIGSSe devices selenized at 500°C for 20 minutes with no alkali addition, 10 nm KF, 20 nm KF, 30 nm NaF+10 nm KF, and 10 nm NaF+20 nm KF.

Figure 8 shows EQE measurements performed at 0 V for KF-only and NaF+KF conditions, while Figure S8 in the Supporting Information shows EQE measurements for NaF-only conditions. Increased EQE response is observed for KF-treated samples compared to the No Alkali baseline condition. Samples that were subjected to both NaF and KF treatments showed significantly higher EQE performance than the bare KF and the baseline conditions. Moreover, the cutoff wavelength in the EQE vs. wavelength plots (Figure 8 and Figure S8) is also altered for the different alkali cases suggesting slightly differing bandgaps between the different alkali cases. Figure S9 in the Supporting Information shows differential quantum efficiency data for each of the conditions considered.⁵² A slight increase in the estimated effective bandgap is observed with alkali treated-

devices (ca. 1.23 eV for the 10 nm KF condition) compared with the No Alkali baseline condition (ca. 1.20 eV). The estimated bandgaps from the differential quantum efficiency data are tabulated in Table S2 in the Supporting Information.

It is apparent from inspection of EQE data in Figures 8 and S8 (Supporting Information) that the decay of EQE in the vicinity of the bandgap is different for the different alkali conditions considered. Application of an Urbach tail model to the EQE data allows characterization of the Urbach Energy E_U . ^{52,53} The Urbach energy characterizes the magnitude of sub-bandgap absorption (band-tailing) in the film. ⁵² Figure S10 in Supporting Information shows a plot of $\ln[-\ln(1-\text{EQE})]$ vs. Energy applied to EQE data for the different conditions considered; estimated Urbach energies extracted from the slope of $\ln[-\ln(1-\text{EQE})]$ vs. Energy plot in the sub-bandgap energy range are tabulated in Table S3 in the Supporting Information. A reduction in band tailing is observed for films treated with alkali (Na and/or K) compared to the No Alkali baseline condition; E_U is reduced from 19.6 meV for the No Alkali case to 13.6-13.8 meV for the NaF and KF treated case. The results presented in Figure S10 and Table S3 suggest reduced defect formation and improvements in the bulk properties of the film as a result of alkali addition.

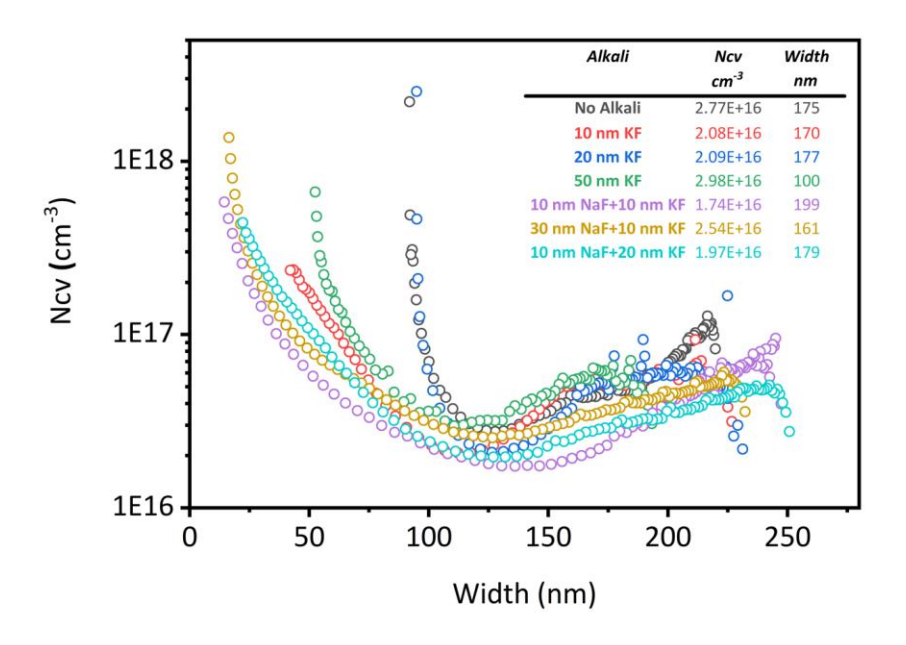


Figure 9: Apparent carrier concentration vs. width from capacitance-voltage measurements of CIGSSe devices selenized with different alkali fluorides thicknesses. Tabulated Ncv values are taken at the minimum of each Ncv-Width curve, and the Width is taken at the 0 V point.

Figure 9 shows the apparent carrier concentration extracted from capacitance-voltage measurements for devices that were subjected to KF treatments and NaF+KF, while Figure S11 in the Supporting Information shows the apparent carrier concentration for devices subjected to NaF treatment only. Despite the varying optoelectronic performance enhancements and increases in the open circuit voltage with Na and K treatments, little change in the absorber carrier concentration was observed. This agrees with multiple reports in the literature where the carrier concentration of solution-processed CISe^{55,56} and CIGSSe⁸ is not influenced appreciably by Na. However, for vacuum-based CIGSe, increases in carrier concentration with Na and K treatments is widely reported. 10,48,54

Conclusion

In this work, the effect of pre-selenization alkali treatments on nanoparticle-based solutionprocessed CIGSSe solar cells was investigated. It was determined that both sodium and potassium enhance CIGSSe grain growth and lead to an increase in coarsened film thickness and a thinner fine-grain material. Additionally, through the use of XPS surface analysis, the presence of an additional Se chemical state at low binding energies was observed for CIGSSe film that had 20 nm KF deposited on prior to selenization, and the film that had undergone a KF post-selenization treatment. This additional Se state is attributed to a K-In-Se surface phase commonly seen in films grown via the 3-stage process and subjected to a KF-PDT. On the other hand, surface Ga and Cu depletion commonly seen in vacuum-based CIGSe films with KF PDT was not observed in films that were selenized with KF added a priori. CIGSSe solar cell optoelectronic performance was found to be significantly enhanced with KF-treatments, with the performance increases being mainly in the open circuit voltage, and to lesser degree in the short-circuit current. Likewise, we also found the Na also enhances CIGSSe device performance by mainly enhancing the short circuit current density. Evaporating both NaF and KF on the as-coated CIGS nanoparticle film, we were able to enhance the performance of CIGSSe solar cell by increasing the power conversion efficiency from 8.8% to 12.0%. In contrast with vacuum-based CIGSe devices, we observed little or no change in the carrier concentration with respect to alkali content in the film. These results demonstrate that KF-treatments and NaF+KF treatments provide an avenue to enhancing the optoelectronic performance of solution-processed CIGSSe solar cells.

Supporting Information

SEM images, EQE data, and C-V data for NaF-only films; x-ray diffraction data; Raman spectroscopy data; Na 1s XPS core level spectra; SEM images of Se 3d and Se LMM – K 2p core level spectra of 20 nm KF-PDT film; light J-V curve for 20 nm KF-PDT device; dark J-V curves for key samples; tabulated series and shunt resistance data; differential EQE data and accompanying extracted bandgap data; Urbach energy data.

Conflicts of Interest

The authors declare no competing financial interests.

Acknowledgments

The authors would like to acknowledge financial support from the National Science Foundation (NSF) under grant #1534691-DMR (DMREF) and #10001536 (INFEWS). E.H.A. also acknowledges support from Kuwait University-Department of Cultural Relations (ID. #15-46014). The authors would like to thank Dr. Dmitry Zemylanov at *Birck Nanotechnology Center, Purdue University* for conducting XPS measurements and for useful discussions. The authors would also like to thank Dr. Xianyi Hu, Joseph Andler, and Jonathan Turnley for preparing Mo-coated soda lime glass substrates used in this work.

References

- (1) Nakamura, M.; Yamaguchi, K.; Kimoto, Y.; Yasaki, Y.; Kato, T.; Sugimoto, H. Cd-Free Cu(In,Ga)(Se,S)₂ Thin-Film Solar Cell With Record Efficiency of 23.35%. *IEEE J. Photovoltaics* **2019**, 1–5.
- Green, M. A.; Hishikawa, Y.; Dunlop, E. D.; Levi, D. H.; Hohl-Ebinger, J.; Ho-Baillie, A.
 W. Y. Solar Cell Efficiency Tables (Version 52). *Prog. Photovoltaics Res. Appl.* 2018, 26 (7), 427–436.
- (3) Kato, T.; Wu, J.-L.; Hirai, Y.; Sugimoto, H.; Bermudez, V. Record Efficiency for Thin-Film Polycrystalline Solar Cells Up to 22.9% Achieved by Cs-Treated Cu(In,Ga)(Se,S)₂. *IEEE J. Photovoltaics* **2019**, *9* (1), 325–330.
- (4) Tai, K. F.; Kamada, R.; Yagioka, T.; Kato, T.; Sugimoto, H. From 20.9 to 22.3% Cu(In,Ga)(S,Se)₂ Solar Cell: Reduced Recombination Rate at the Heterojunction and the Depletion Region Due to K-Treatment. *Jpn. J. Appl. Phys.* **2017**, *56* (8S2), 08MC03.
- (5) Jackson, P.; Hariskos, D.; Wuerz, R.; Wischmann, W.; Powalla, M. Compositional Investigation of Potassium Doped Cu(In,Ga)Se₂ Solar Cells with Efficiencies up to 20.8%. Phys. Status Solidi - Rapid Res. Lett. 2014, 8 (3), 219–222.
- (6) Wolden, C. A.; Kurtin, J.; Baxter, J. B.; Repins, I.; Shaheen, S. E.; Torvik, J. T.; Rockett, A. A.; Fthenakis, V. M.; Aydil, E. S. Photovoltaic Manufacturing: Present Status, Future Prospects, and Research Needs. J. Vac. Sci. Technol. A Vacuum, Surfaces, Film. 2011, 29 (3), 030801.
- McLeod, S. M.; Hages, C. J.; Carter, N. J.; Agrawal, R. Synthesis and Characterization of
 15% Efficient CIGSSe Solar Cells from Nanoparticle Inks. *Prog. Photovoltaics Res. Appl.* 2015, 23 (11), 1550–1556.

- (8) Guo, Q.; Ford, G. M.; Agrawal, R.; Hillhouse, H. W. Ink Formulation and Low-Temperature Incorporation of Sodium to Yield 12% Efficient Cu(In,Ga)(S,Se)₂ Solar Cells from Sulfide Nanocrystal Inks. *Prog. Photovoltaics Res. Appl.* 2013, 21 (1), 64–71.
- (9) Zhang, T.; Yang, Y.; Liu, D.; Tse, S. C.; Cao, W.; Feng, Z.; Chen, S.; Qian, L. High Efficiency Solution-Processed Thin-Film Cu(In,Ga)(Se,S)₂ Solar Cells. *Energy Environ. Sci.* **2016**, *9* (12), 3674–3681.
- (10) Nakada, T.; Iga, D.; Ohbo, H.; Kunioka, A. Effects of Sodium on Cu(In,Ga)Se₂-Based Thin Films and Solar Cells. *Jpn. J. Appl. Phys.* **1997**, *36* (Part 1, No. 2), 732–737.
- (11) Kronik, L.; Cahen, D.; Schock, H. W. Effects of Sodium on Polycrystalline Cu(In,Ga)Se₂ and Its Solar Cell Performance. *Adv. Mater.* **2002**, *10* (1), 31–36.
- (12) Granath, K.; Bodegård, M.; Stolt, L. The Effect of NaF on Cu(In,Ga)Se₂ Thin Film Solar Cells. Sol. Energy Mater. Sol. Cells **2000**, 60 (3), 279–293.
- (13) Zhao, X.; Lu, M.; Koeper, M. J.; Agrawal, R. Solution-Processed Sulfur Depleted Cu(In,Ga)Se₂ Solar Cells Synthesized from a Monoamine–Dithiol Solvent Mixture. *J. Mater. Chem. A* 2016, 4 (19), 7390–7397.
- (14) Mungan, E. S.; Wang, X.; Alam, M. A. Modeling the Effects of Na Incorporation on CIGS Solar Cells. *IEEE J. Photovoltaics* **2013**, *3* (1), 451–456.
- (15) Stanbery, B. J.; Kincal, S.; Kim, S.; Anderson, T. J.; Crisalle, O. D.; Ahrenkiel, S. P.; Lippold, G. Role of Sodium in the Control of Defect Structures in CIS [Solar Cells]. In Conference Record of the Twenty-Eighth IEEE Photovoltaic Specialists Conference -2000 (Cat. No.00CH37036); IEEE, 2000; Vol. 2000, pp 440–445.
- (16) Ruckh, H.; Schmid, D.; Kaiser, M.; Schaffler, R.; Walter, T.; Schock, H. W. Influence of Substrates on the Electrical Properties of Cu(In,Ga)Se₂ Thin Films. In *Proceedings of*

- 1994 IEEE 1st World Conference on Photovoltaic Energy Conversion WCPEC (A Joint Conference of PVSC, PVSEC and PSEC); IEEE, 1996; Vol. 1, pp 156–159.
- (17) Rudmann, D. Effects of Sodium on Growth and Properties of Cu(In, Ga)Se₂ Thin Films and Solar Cells, Eidgenössische Technische Hochschule ETH Zürich, 2004.
- (18) McLeod, S.; Alruqobah, E.; Agrawal, R. Liquid Assisted Grain Growth in Solution Processed Cu(In,Ga)(S,Se)₂. *Sol. Energy Mater. Sol. Cells* **2019**, *195* (February), 12–23.
- (19) Bodeg Ård, M.; Granath, K.; Stolt, L. Growth of Cu(In,Ga)Se₂ Thin Films by Coevaporation Using Alkaline Precursors. *Thin Solid Films* **2000**, *361–362*, 9–16.
- (20) Contreras, M. A.; Egaas, B.; Dippo, P.; Webb, J.; Granata, J.; Ramanathan, K.; Asher, S.; Swartzlander, A.; Noufi, R. On the Role of Na and Modifications to Cu(In,Ga)Se₂
 Absorber Materials Using Thin-MF (M=Na, K, Cs) Precursor Layers [Solar Cells]. In Conference Record of the Twenty Sixth IEEE Photovoltaic Specialists Conference 1997; IEEE, 1997; Vol. 96, pp 359–362.
- (21) Chirilă, A.; Reinhard, P.; Pianezzi, F.; Bloesch, P.; Uhl, A. R.; Fella, C.; Kranz, L.; Keller, D.; Gretener, C.; Hagendorfer, H.; Jaeger, D.; Erni, R.; Nishiwaki, S.; Buecheler, S.; Tiwari, A. N. Potassium-Induced Surface Modification of Cu(In,Ga)Se₂ Thin Films for High-Efficiency Solar Cells. *Nat. Mater.* 2013, 12 (12), 1107–1111.
- (22) Avancini, E.; Carron, R.; Weiss, T. P.; Andres, C.; Bürki, M.; Schreiner, C.; Figi, R.; Romanyuk, Y. E.; Buecheler, S.; Tiwari, A. N. Effects of Rubidium Fluoride and Potassium Fluoride Postdeposition Treatments on Cu(In,Ga)Se₂ Thin Films and Solar Cell Performance. *Chem. Mater.* **2017**, *29* (22), 9695–9704.
- (23) Chantana, J.; Kawano, Y.; Nishimura, T.; Kimoto, Y.; Kato, T.; Sugimoto, H.; Minemoto, T. Effect of Alkali Treatment on Photovoltaic Performances of Cu(In,Ga)(S,Se)₂ Solar

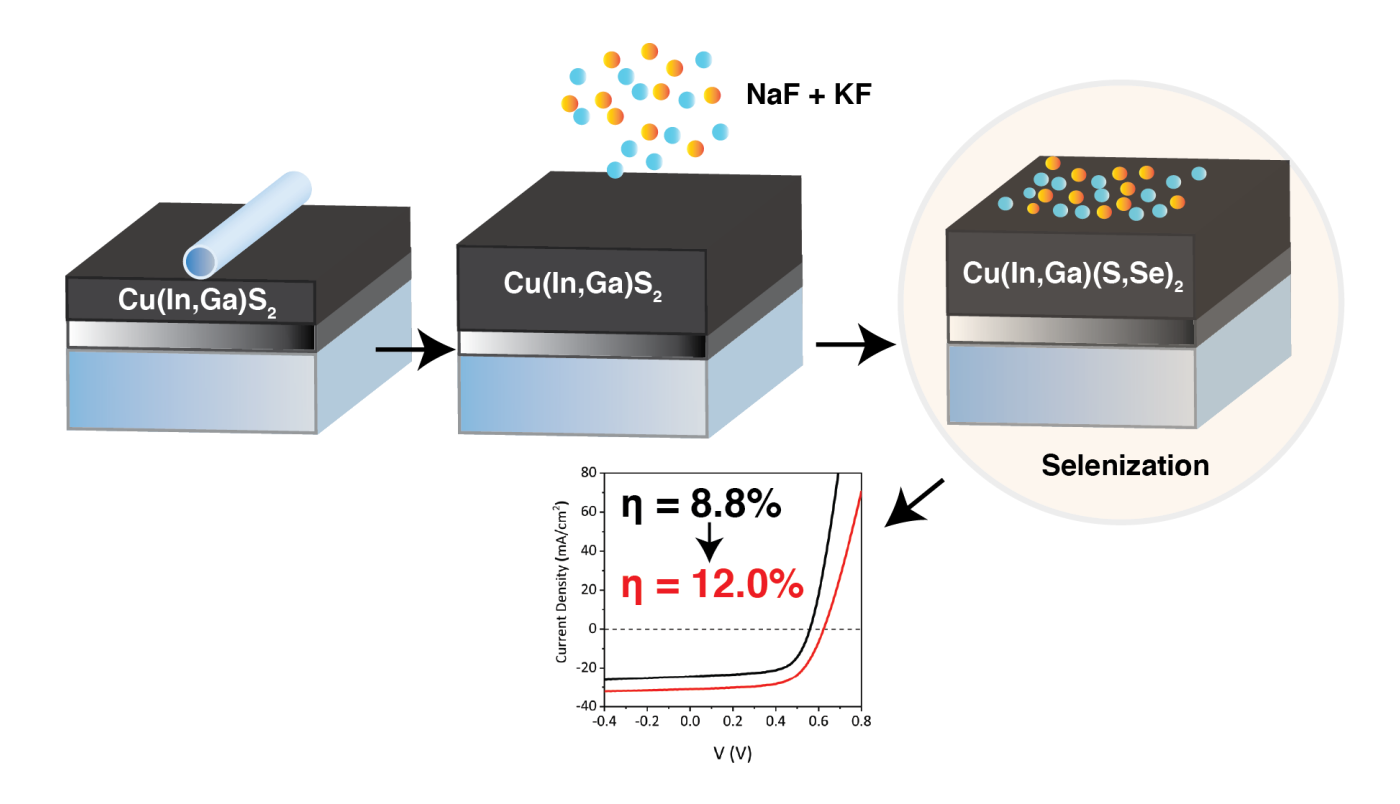
- Cells and Their Absorber Quality Analyzed by Urbach Energy and Carrier Recombination Rates. *ACS Appl. Energy Mater.* **2020**, *3* (2), 1292–1297.
- (24) Handick, E.; Reinhard, P.; Wilks, R. G.; Pianezzi, F.; Kunze, T.; Kreikemeyer-Lorenzo, D.; Weinhardt, L.; Blum, M.; Yang, W.; Gorgoi, M.; Ikenaga, E.; Gerlach, D.; Ueda, S.; Yamashita, Y.; Chikyow, T.; Heske, C.; Buecheler, S.; Tiwari, A. N.; Bär, M. Formation of a K-In-Se Surface Species by NaF/KF Postdeposition Treatment of Cu(In,Ga)Se₂ Thin-Film Solar Cell Absorbers. ACS Appl. Mater. Interfaces 2017, 9 (4), 3581–3589.
- (25) Pistor, P.; Greiner, D.; Kaufmann, C. A.; Brunken, S.; Gorgoi, M.; Steigert, A.; Calvet, W.; Lauermann, I.; Klenk, R.; Unold, T.; Lux-Steiner, M. C. Experimental Indication for Band Gap Widening of Chalcopyrite Solar Cell Absorbers after Potassium Fluoride Treatment. Appl. Phys. Lett. 2014, 105 (6).
- (26) Siebentritt, S.; Avancini, E.; Bär, M.; Bombsch, J.; Bourgeois, E.; Buecheler, S.; Carron, R.; Castro, C.; Duguay, S.; Félix, R.; Handick, E.; Hariskos, D.; Havu, V.; Jackson, P.; Komsa, H.; Kunze, T.; Malitckaya, M.; Menozzi, R.; Nesladek, M.; Nicoara, N.; Puska, M.; Raghuwanshi, M.; Pareige, P.; Sadewasser, S.; Sozzi, G.; Tiwari, A. N.; Ueda, S.; Vilalta-Clemente, A.; Weiss, T. P.; Werner, F.; Wilks, R. G.; Witte, W.; Wolter, M. H. Heavy Alkali Treatment of Cu(In,Ga)Se₂ Solar Cells: Surface versus Bulk Effects. Adv. Energy Mater. 2020, 10 (8), 1903752.
- (27) Malitckaya, M.; Komsa, H.-P.; Havu, V.; Puska, M. J. Effect of Alkali Metal Atom Doping on the CuInSe₂-Based Solar Cell Absorber. *J. Phys. Chem. C* **2017**, *121* (29), 15516–15528.
- (28) Handick, E.; Reinhard, P.; Alsmeier, J. H.; Köhler, L.; Pianezzi, F.; Krause, S.; Gorgoi, M.; Ikenaga, E.; Koch, N.; Wilks, R. G.; Buecheler, S.; Tiwari, A. N.; Bär, M. Potassium

- Postdeposition Treatment-Induced Band Gap Widening at Cu(In,Ga)Se₂ Surfaces Reason for Performance Leap? *ACS Appl. Mater. Interfaces* **2015**, *7* (49), 27414–27420.
- (29) Schneider, C. A.; Rasband, W. S.; Eliceiri, K. W. NIH Image to ImageJ: 25 Years of Image Analysis. *Nat. Methods* **2012**, *9* (7), 671–675.
- (30) Hauschild, D.; Meyer, F.; Pohlner, S.; Lechner, R.; Dietmüller, R.; Palm, J.; Heske, C.; Weinhardt, L.; Reinert, F. Impact of Environmental Conditions on the Chemical Surface Properties of Cu(In,Ga)(S,Se)₂ Thin-Film Solar Cell Absorbers. *J. Appl. Phys.* 2014, 115 (18), 183707.
- (31) Hegedus, S. S.; Shafarman, W. N. Thin-Film Solar Cells: Device Measurements and Analysis. *Prog. Photovoltaics Res. Appl.* **2004**, *12* (2–3), 155–176.
- (32) Zhao, D.; Fan, Q.; Tian, Q.; Zhou, Z.; Meng, Y.; Kou, D.; Zhou, W.; Wu, S. Eliminating Fine-Grained Layers in Cu(In,Ga)(S,Se)₂ Thin Films for Solution-Processed High Efficiency Solar Cells. *J. Mater. Chem. A* **2016**, *4* (35), 13476–13481.
- (33) Hages, C. J.; Koeper, M. J.; Agrawal, R. Optoelectronic and Material Properties of Nanocrystal-Based CZTSe Absorbers with Ag-Alloying. Sol. Energy Mater. Sol. Cells 2016, 145, 342–348.
- (34) Guo, Q.; Ford, G. M.; Hillhouse, H. W.; Agrawal, R. Sulfide Nanocrystal Inks for Dense Cu(In_{1-x}Ga_x)(S_{1-y}Se_y)₂ Absorber Films and Their Photovoltaic Performance. *Nano Lett.* **2009**, *9* (8), 3060–3065.
- (35) Chernomordik, B. D.; Béland, A. E.; Deng, D. D.; Francis, L. F.; Aydil, E. S.
 Microstructure Evolution and Crystal Growth in Cu₂ZnSnS₄ Thin Films Formed by
 Annealing Colloidal Nanocrystal Coatings. Chem. Mater. 2014, 26 (10), 3191–3201.
- (36) Williams, B. A.; Smeaton, M. A.; Trejo, N. D.; Francis, L. F.; Aydil, E. S. Effect of

- Nanocrystal Size and Carbon on Grain Growth during Annealing of Copper Zinc Tin Sulfide Nanocrystal Coatings. *Chem. Mater.* **2017**, *29* (4), 1676–1683.
- (37) Sutter-Fella, C. M.; Stückelberger, J. A.; Hagendorfer, H.; La Mattina, F.; Kranz, L.; Nishiwaki, S.; Uhl, A. R.; Romanyuk, Y. E.; Tiwari, A. N. Sodium Assisted Sintering of Chalcogenides and Its Application to Solution Processed Cu₂ZnSn(S,Se)₄ Thin Film Solar Cells. *Chem. Mater.* **2014**, *26* (3), 1420–1425.
- (38) Braunger, D.; Hariskos, D.; Bilger, G.; Rau, U.; Schock, H. W. Influence of Sodium on the Growth of Polycrystalline Cu(In,Ga)Se₂ Thin Films. *Thin Solid Films* **2000**, *361*, 161–166.
- (39) Uhl, A. R.; Fuchs, P.; Rieger, A.; Pianezzi, F.; Sutter-Fella, C. M.; Kranz, L.; Keller, D.; Hagendorfer, H.; Romanyuk, Y. E.; LaMattina, F.; Yoon, S.; Karvonen, L.; Magorian-Friedlmeier, T.; Ahlswede, E.; VanGenechten, D.; Stassin, F.; Tiwari, A. N. Liquid-Selenium-Enhanced Grain Growth of Nanoparticle Precursor Layers for CuInSe₂ Solar Cell Absorbers. *Prog. Photovoltaics Res. Appl.* 2015, 23 (9), 1110–1119.
- (40) Hages, C. J.; Koeper, M. J.; Miskin, C. K.; Brew, K. W.; Agrawal, R. Controlled Grain Growth for High Performance Nanoparticle-Based Kesterite Solar Cells. *Chem. Mater.* 2016, 28 (21), 7703–7714.
- (41) Lepetit, T.; Harel, S.; Arzel, L.; Ouvrard, G.; Barreau, N. KF Post Deposition Treatment in Co-Evaporated Cu(In,Ga)Se₂ Thin Film Solar Cells: Beneficial or Detrimental Effect Induced by the Absorber Characteristics. *Prog. Photovoltaics Res. Appl.* 2017, 25 (12), 1068–1076.
- (42) Witte, W.; Kniese, R.; Powalla, M. Raman Investigations of Cu(In,Ga)Se₂ Thin Films with Various Copper Contents. *Thin Solid Films* **2008**, *517* (2), 867–869.

- (43) Canava, B.; Vigneron, J.; Etcheberry, A.; Guillemoles, J. .; Lincot, D. High Resolution XPS Studies of Se Chemistry of a Cu(In,Ga)Se₂ Surface. *Appl. Surf. Sci.* **2002**, *202* (1–2), 8–14.
- (44) Lepetit, T.; Harel, S.; Arzel, L.; Ouvrard, G.; Barreau, N. Coevaporated KInSe₂: A Fast Alternative to KF Postdeposition Treatment in High-Efficiency Cu(In,Ga)Se₂ Thin Film Solar Cells. *IEEE J. Photovoltaics* **2016**, *6* (5), 1316–1320.
- (45) Clark, J. A.; Uhl, A. R.; Martin, T. R.; Hillhouse, H. W. Evolution of Morphology and Composition during Annealing and Selenization in Solution-Processed Cu₂ZnSn(S,Se)₄. *Chem. Mater.* **2017**, acs.chemmater.7b03313.
- (46) Nicoara, N.; Harel, S.; Lepetit, T.; Arzel, L.; Barreau, N.; Sadewasser, S. Impact of KF Post-Deposition Treatment on Aging of the Cu(In,Ga)Se₂ Surface and Its Interface with CdS. ACS Appl. Energy Mater. 2018, 1 (6), 2681–2688.
- (47) Mezher, M.; Mansfield, L. M.; Horsley, K.; Blum, M.; Wieting, R.; Weinhardt, L.;
 Ramanathan, K.; Heske, C. KF Post-Deposition Treatment of Industrial Cu(In, Ga)(S,Se)₂
 Thin-Film Surfaces: Modifying the Chemical and Electronic Structure. *Appl. Phys. Lett.* 2017, 111 (7), 071601.
- (48) Pianezzi, F.; Reinhard, P.; Chirilă, A.; Bissig, B.; Nishiwaki, S.; Buecheler, S.; Tiwari, A. N. Unveiling the Effects of Post-Deposition Treatment with Different Alkaline Elements on the Electronic Properties of CIGS Thin Film Solar Cells. *Phys. Chem. Chem. Phys.* 2014, 16 (19), 8843–8851.
- (49) Kodalle, T.; Heinemann, M. D.; Greiner, D.; Yetkin, H. A.; Klupsch, M.; Li, C.; van Aken, P. A.; Lauermann, I.; Schlatmann, R.; Kaufmann, C. A. Elucidating the Mechanism of an RbF Post Deposition Treatment in CIGS Thin Film Solar Cells. *Sol. RRL* **2018**, *2*

- (9), 1800156.
- (50) Villanueva-Tovar, A.; Kodalle, T.; Kaufmann, C. A.; Schlatmann, R.; Klenk, R. Limitation of Current Transport across the Heterojunction in Cu(In,Ga)Se₂ Solar Cells Prepared with Alkali Fluoride Postdeposition Treatment. Sol. RRL 2020, 4 (4), 1900560.
- (51) Mezher, M.; Mansfield, L. M.; Horsley, K.; Yang, W.; Blum, M.; Weinhardt, L.; Ramanathan, K.; Heske, C. Variations in the Chemical and Electronic Impact of Post-Deposition Treatments on Cu(In,Ga)(S,Se)₂ Absorbers. ACS Appl. Energy Mater. 2019, 2 (12), 8641–8648.
- (52) Hages, C. J.; Carter, N. J.; Agrawal, R. Generalized Quantum Efficiency Analysis for Non-Ideal Solar Cells: Case of Cu₂ZnSnSe₄. *J. Appl. Phys.* **2016**, *119* (1), 014505.
- (53) Troviano, M.; Taretto, K. Analysis of Internal Quantum Efficiency in Double-Graded Bandgap Solar Cells Including Sub-Bandgap Absorption. Sol. Energy Mater. Sol. Cells 2011, 95 (3), 821–828.
- (54) Wang, S.; Hao, X.; Islam, M. M.; Kato, T.; Sugimoto, H.; Akimoto, K.; Sakurai, T.
 Influence of Potassium Treatment on Electronic Properties of Cu(In_{1-x}Ga_x)(Se_{1-y}S_y)₂ Solar
 Cells Studied by Steady State Photo-Capacitance and Admittance Spectroscopy. *Jpn. J.*Appl. Phys. 2018, 57 (8S3), 08RC13.
- (55) Rehan, S.; Moon, J.; Kim, T. G.; Gwak, J.; Kim, J.; Kim, J. W.; Jo, W.; Ahn, S. K.; Ahn, S. Role of Na in Solution-Processed CuInSe₂ (CISe) Devices: A Different Story for Improving Efficiency. *Nano Energy* 2018, 48 (March), 401–412.
- (56) Moon, J.; Rehan, S.; Rana, T. R.; Byungsung, O.; Ahn, S. K.; Ahn, S. Na-induced Conversion of a Notorious Fine-Grained Residue Layer into a Working Absorber in Solution-Processed CuInSe₂ Devices. *Sol. RRL* **2019**, *1900260*, 1–10.



FOR GRAPHICAL ABSTRACT